Comparative investigation of microstructure and properties of Ni-coated FeSiAl soft magnetic composite coatings produced by cold spraying and HVOF

Xinliang Xie, Chaoyue Chen, Yingchun Xie, Eric Aubry, Zhongming Ren, Gang Ji, Hanlin Liao

Version of Record: https://www.sciencedirect.com/science/article/pii/S0257897218313896
Manuscript_ec520e9e650eef8dbfd31597e8eabbd1

Comparative investigation of microstructure and properties of Ni-coated FeSiAl soft magnetic composite coatings produced by cold spraying and HVOF

Xinliang XIE[1,3], Chaoyue CHEN[1,2*], Yingchun XIE[4], Eric AUBRY[5], Zhongming REN[2], Gang JI[3], Hanlin LIAO[1]

1. *ICB UMR 6303, CNRS, Univ. Bourgogne Franche-Comté, UTBM, F-90010 Belfort, France*
2. *State Key Laboratory of Advanced Special Steels, School of Materials Science and Engineering, Shanghai University, Shanghai 200444, China*
3. *Unité Matériaux et Transformations, CNRS UMR 8207, Université Lille 1, Villeneuve d'Ascq, 59655, France*
4. *National Engineering Laboratory for Modern Materials Surface Engineering Technology; The Key Lab of Guangdong for Modern Surface Engineering Technology; Guangdong Institute of New Materials, Guangzhou 510651, P.R. China*
5. *Nipson Technology, 12 Avenue des Trois Chênes, 90000 Belfort, France*

Abstract: In this work, the techniques of cold spray (CS) and high velocity oxygen-fuel (HVOF) were employed to fabricate Ni/FeSiAl soft magnetic composite (SMC) coatings by using Ni-coated FeSiAl composite powder. The microstructural features were characterized in terms of scanning electron microscope (SEM) and X-ray diffraction (XRD) analyses. The tribological and magnetic properties of the Ni/FeSiAl SMC coatings were also comparatively studied. Results showed that the CS coating exhibited higher particle deformation and much higher density, whereas the HVOF coating showed more visible defects and slightly higher oxide content. Both CS coating and HVOF coating resulted some loss of FeSiAl particles during deposition, while a higher content of FeSiAl particles was achieved in the HVOF composite coating, indicated a higher deposition efficiency of FeSiAl particles during HVOF deposition. According to the XRD analysis, both SMC coatings had no obvious oxidation and phase transformation during deposition processes. The EDS analysis proved partially melted particles during HVOF deposition. Tribological tests revealed a better wear performance of the CS coating as a result of the enhanced plastic deformation and microhardness. The HVOF coating showed a better magnetic performance, with a lower coercivity and a higher saturation magnetization compared to those of CS coating. This can be explained by a higher retainability of FeSiAl particles and a smaller strain stress generation during HVOF deposition.

Keywords: Cold spraying; HVOF; Soft magnetic composites; FeSiAl alloy; Cladded powder

* Corresponding author: Chaoyue CHEN, email: cchen1@shu.edu.cn

1. Introduction

In recent years, soft magnetic composites (SMCs) exhibit enormous advantages and have a substantial impact on electric-magnetic switching device for their high electrical resistivity, low eddy current loss at high frequency, a low anisotropy constant and low coercivity [1-3]. Up to now, various material systems of SMCs have been studied in the literature, such as Fe-Si [4], Fe-Ni [5], Fe-Si-Al [6-8], Fe-Ni-Mo [9] and Fe-Cu-Nb-Si-B [10]. Among them, FeSiAl based SMCs are significant for many applications including transformers, electric motors, sensors and inductors due to their excellent magnetic properties [11, 12]. Traditionally, the most common technique for the production of SMCs is powder metallurgy procedures including insulation coating, addition of binding agents, compaction and annealing [13, 14]. However, the powder metallurgy processes are limited to the production of magnetic cores or parts but inapplicable for fabricating thin SMC coatings.

Thermal spraying is a major surface modification technique, which consists of a complete or partial melting of feedstock material, an acceleration of the particles and their subsequent impact onto a coated part, where the particles rapidly solidify and form a lamellar structure. Recently, various studies have been reported on the fabrication of soft magnetic coatings via different thermal spray techniques, such as atmosphere plasma spraying (APS) [15-18], high-velocity oxy-fuel (HVOF) [5, 19, 20] and twin arc spraying [21]. For example, S.J Dong et al [15]fabricated FeSiB soft magnetic coating with improved saturation magnetization using APS process combined with the dry-ice blasting. M. Cherigui et.al [19, 20, 22] studied the diagnostic, structure, and magnetic properties of FeSi based coatings deposited by HVOF using microcrystalline powders. These fabricated coatings showed a soft magnetic property. However, during thermal processes, soft magnetic particles were exposed to fuel gases or atmosphere, which led to serious oxidation and corrosion [19]. Consequently, the magnetic performance of the thermal sprayed coatings was weakened. Besides, the limited deformation of these hard FeSi-based particles resulted in high porosities in the thermal sprayed coatings [5], which also weakened their mechanical and magnetic properties.

As a new emerging technique, cold spraying (CS), provides an effective approach to produce high quality metallic coatings through the solid-state deposition. A coating is formed

through intensive plastic deformation of particles impacting on a substrate at a temperature well below the melting point of the spray material. Unlike the conventional thermal spray processes, cold sprayed coating is formed through the mechanical interlocking and metallurgical bonding of the solid-state particles [23, 24]. Therefore, CS is particularly suitable to deposit coatings of thermosensitive materials without any significant phase change and oxidation of feedstocks [25-27]. Up to now, very few attempts have been made to fabricate soft magnetic coatings via CS. M. Cherigui.et.al [25] fabricated FeSiBNbCu-Al composite coating via CS of nanostructured powders mixed with Al powders. The as-sprayed coatings presented a soft ferromagnetic property despite the presence of nonmagnetic Al [25]. However, the addition of a nonmagnetic Al layer greatly reduces the overall magnetic permeability, which yields a problematic balance of properties [5]. According to the work of W.Y Li [26], nanostructured Fe-Si coatings were deposited by using the mechanically milled powders as feedstock. The fabricated Fe-Si coating exhibited a high coercivity (190 kA/m) and had a great potential for the application of magnetic recording materials [26].

In this work, both the HVOF and CS deposition techniques were employed to fabricate Ni/FeSiAl SMC coatings. To produce high quality SMC coatings, a novel FeSiAl composite powder decorated by a Ni layer was used as feedstock. There are three main reasons for choosing Ni as the matrix phase: firstly, Ni is a soft magnetic material and its excellent ductility makes it an ideal binder material, which can favor the deposition of FeSiAl particles, especially in the CS process. Secondly, Ni shows a relatively high resistance to corrosion, therefore, it acts as a thin protective layer preventing the core FeSiAl particles from oxidation during HVOF deposition. At last, its high corrosion and wear resistance make the deposited coatings suitable for the application in corrosion situations. Thus, in this study, the microstructure, oxidation behavior, phase transformation as well as the deposition mechanisms of CS and HVOF coatings were comparatively investigated. Their mechanical and magnetic properties related to the microstructure were also investigated.

2. Experimental details

2.1 Materials and methods

The commercial gas atomized Fe-9.6Si-5.4Al (in wt.%) powder that was pre-coated with

a Ni layer via hydrometallurgy process (Beijing General Research Institute of Nonferrous Metals, China) was selected as the feedstock material to fabricate Ni/FeSiAl SMC coatings. Ni-coated FeSiAl particles were produced by hydrothermal hydrogen reduction process, where Ni was reduced from nickel sulfate-ammonia solution by hydrogen at a temperature of 150 °C in autoclaves [28, 29]. The surface morphology and size distribution of the Ni-coated FeSiAl powders are given in Figs. 1a and b, respectively. As shown in Fig. 1a, the composite powder exhibits a spherical morphology with an average particle size of around 56 µm according to a laser diffraction sizer (Mastersizer 2000, Malvern Instruments Ltd., UK). The cross-sectional images of the Ni-coated FeSiAl particles are given Figs. 1 c and d. It can be noticed that the FeSiAl core is uniformly coated by a Ni layer with a thickness of 3-5 µm, which can facilitate the deposition of FeSiAl particle in the composite coating. The pure Al plates after grit-blasting were used as substrates in both CS and HVOF processes.

The CS and HVOF deposition techniques were employed to fabricate Ni/FeSiAl composite coatings. The CS deposition was performed in a homemade CS system (LERMPS, UTBM, France) with an optimal de-Laval-type converging-diverging nozzle. High pressure compressed air was used as powder carrier gas and propelling gas. Based on previous studies [30], the optimal processing parameters for CS deposition are chosen and listed in Table 1. Nozzle trajectory was repeated for 20 times to obtain a thick coating. HVOF spray experiments were carried out in a commercial diamond jet spraying system (DJ2702) operating with methane and oxygen as combustion gases. N_2 was used as the powder carrier gas. Other main processing parameters are listed in Table 2. Since the HVOF process has a relative higher deposition efficiency than CS, the nozzle trajectory for HVOF deposition was repeated 10 times.

2.2 Material characterization

The feedstock and coatings were examined by an X-Ray diffractometer system (Siemens D500, Germany) operating at 40 kV with the Co (λ =1.78897 Å) source and scan step of 0.02°. A scanning electron microscope (SEM) equipped with EDX unit (Carl Zeiss ULTRA, Germany) was used for the coating and powder observation and element analysis. Energy dispersive spectroscopy [31] [31] analysis was also carried out to evaluate the oxide content

of the as-sprayed coatings. The porosity and FeSiAl content in the initial powder and coatings were evaluated by image analysis software (ImageJ, NIH, Bethesda, Md.) based on five SEM images. The flattening ratios of FeSiAl particle in the initial powder and the coatings were obtained by measuring the longest length of the particle over the shortest one. For flattening ratio measurement, an average value was obtained from a minimum of 40 FeSiAl particles per sample.

The coating microhardness was measured by a Vickers hardness indenter (Leitz, Germany) with a load of 100 g for 15 s. 10 positions were randomly tested and averaged to determine the microhardness. Dry sliding tribological tests were performed on a ball-on-disc CSEM tribometer in an ambient environment (temperature: ~25°C, humidity: 40-60 %). Before tribological tests, all the samples were polished to the same roughness (about Ra=0.5 μm). A WC-Co pin ball in 6 mm diameter was used as a counterpart under a constant load of 5 N. The sliding velocity and ultimate sliding distance were 10 cm/s and 300 m, respectively. After friction test, the surface of worn samples was observed and analyzed by SEM and EDS. The wear rates of the samples were calculated according to the cross-sectional profiles of worn track measured by an Altisurf 500 profilometer (France).

The magnetic measurements for the powders and the SMC coatings were carried out with a VSM Lakeshore (model 7300) at ambient temperature. Before magnetic property measurements, the 10 mm×10 mm cut samples were placed in sodium hydroxide solution for several hours to fully dissolve the Al substrates; while SMC coatings were well preserved after corrosion. The SMC samples were then grounded to remove the surface oxide films.

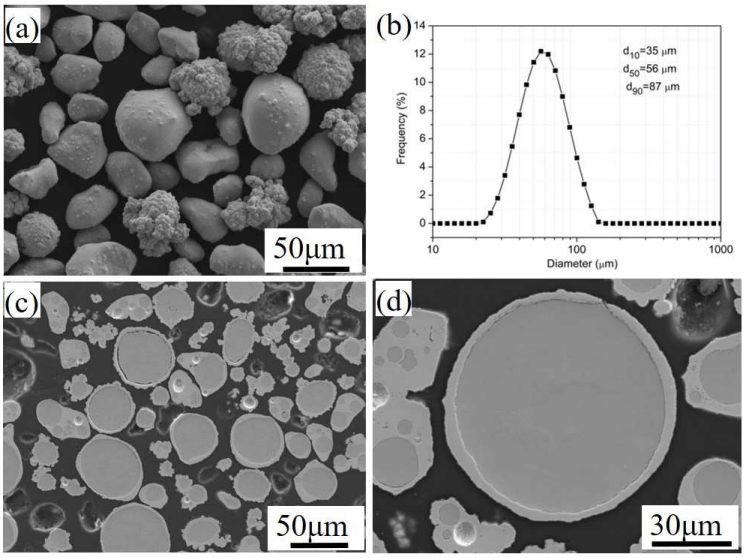

Fig. 1 (a) Surface morphology of the Ni-coated FeSiAl composite powder, (b) particle size distribution, (c) and (d) the cross-sectional views of the core-shell composite particle at different magnifications.

Table 1 Main processing paramaters for CS deposition.

Propelling gas temperature	620 ℃
Propelling gas pressure	3.0 MPa
Scanning velocity	100 mm/s
Spray distance	30 mm
Carrier gas pressure	3.0 MPa
Powder feed rate	24 g/min
Scanning step	2 mm

Table 2 Main processing paramaters for HVOF deposition.

Methane fuel flow rate	180 NL/min
Oxygen gas flow rate	420 NL/min
Scanning velocity	400 μm/s
Spray distance	280 mm
Powder feed rate	35 g/min
Scanning step	8 mm

3. Results and Discussion

3.1 Phase composition

Fig. 2a demonstrates the XRD patterns of initial powder, CS and HVOF composite coatings. The initial powder contains Ni and $Al_{0.3}Si_{0.7}Fe_3$ phases. It can be noticed that the peaks of Ni phase are much stronger than those of $Al_{0.3}Si_{0.7}Fe_3$ phase even though the volume fraction of Ni (40 vol.%) is lower than that of $Al_{0.3}Si_{0.7}Fe_3$ (60 vol.%) in the initial powder. This is due to the depth limitation of X-ray diffraction (~10 μm) and the core-shell structure of the feedstock powder, where most of the X-rays are diffracted by the Ni shell layers (several microns). In both SMC coatings, no other potential phases such as oxides are detectable besides the main phases of Ni and $Al_{0.3}Si_{0.7}Fe_3$, indicating that neither significant chemical reaction nor phase transformation occurred during CS and HVOF deposition. According to Ref [32], FeSiAl alloy can exhibit three major phases including A_2, B_2 and DO_3. Both the initial powder and composite coatings in this study presented DO_3 structure ($Al_{0.3}Si_{0.7}Fe_3$). As indicated in Ref [32, 33], the phase transformation from ordered DO_3 structure to disordered A_2 and B_2 structure could take place after high energy ball milling of the FeSiAl powder. No phase transformation was observed during both the CS and HVOF processes in this study. Obviously, the low temperature feature of CS deposition can prevent the composite particle from oxidation or phase transformation. As for the HVOF process, despite the relatively high processing temperature and the oxygen atmosphere, oxides were not detected via XRD patterns in this work, showing the limited oxidation of the composite particles. However, oxides were detected in the conventional HVOF sprayed FeSi and FeNb coatings reported by M. Cherigui et.al, where the particles were partially melted and exposed to combustion gases in the process [20, 22]. By using Ni-coated FeSiAl powder, the melting and oxidation of the core FeSiAl particles can be largely decreased due to the presence of Ni layer during HVOF process. The microstructure and composition characterization of the coatings will be carried out to support this point in the following section.

Fig. 2b shows the detailed XRD spectra of the 2θ angle between 50° and 55°. It can be observed that the Ni (111) and $Al_{0.3}Si_{0.7}Fe_3$ (110) diffraction peaks of both coatings slightly shifted to higher angles in comparison with the initial powder. However, the peaks of CS coating display a greater shift compared to those of HVOF coating. This can be explained by greater plastic deformation of impact particle with higher in-flight velocity. These highly deformed particles can lead to the formation of lattice defects and residual stress, resulting in

a peak shift in the XRD pattern [30, 34]. Besides, the $Al_{0.3}Si_{0.7}Fe_3$ (110) peak intensities in both deposited coatings decreased compared to those of initial powder, which may be attributed to the loss of FeSiAl particles during deposition processes. However, a lower intensity of FeSiAl phase in CS coating than that of HVOF suggests more serious FeSiAl loss during CS deposition.

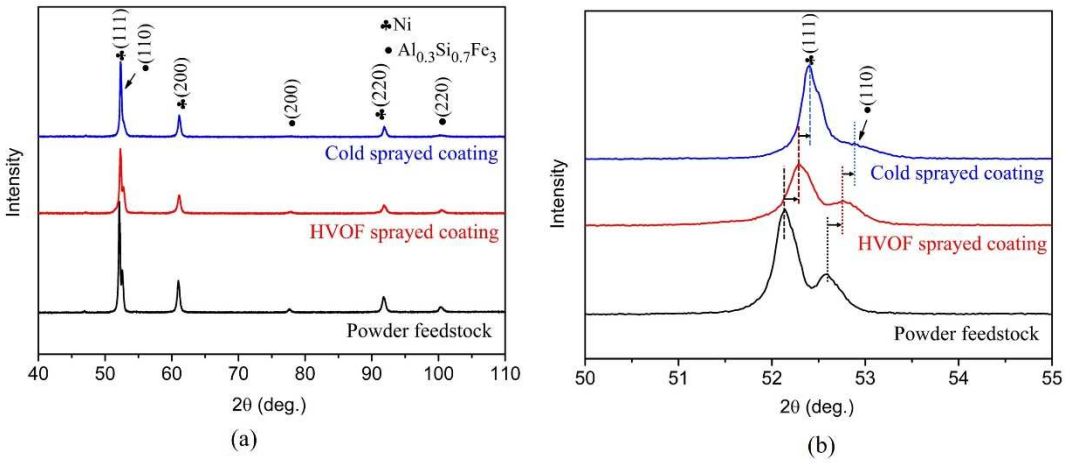

Fig. 2 (a) XRD analysis of the initial powder, CS and HVOF composite coatings; (b) the detailed XRD spectra of the 2θ angle between 50° and 55°.

3.2 Coating microstructure

The cross-sectional microstructure of the composite coatings fabricated by CS and HVOF are given in Fig. 3a and Fig. 3d, respectively. In Fig. 3a, the CS composite coating exhibits high density and crack-free features with a thickness of ~325 μm. At the coating/substrate interface, the intimate bonding with the Al substrate can be observed without obvious cracks. Statistical analysis based on the cross-sectional SEM images yields an extremely low porosity of ~ 0.6%. The FeSiAl particles are uniformly distributed in the CS coating except that some big FeSiAl particles can be found near the coating/substrate interface.

As shown in the magnified images in Figs. 3b and c, FeSiAl particles are intimately bonded with the ductile Ni layers without any gaps. As verified by the EDS mapping in Fig. 4, Ni and the elements of FeSiAl phase are clearly separated without formation of any mixed phases. The volume fraction of FeSiAl particles in CS coating was calculated to be about 25%, which is less than half of that in the initial powder (62%). It indicates that a large number of

FeSiAl particles rebound away during the coating build-up process, which is in a good agreement with the decreasing intensity in XRD results. In addition, the FeSiAl particles are highly deformed and elongated at the direction perpendicular to the deposition. The flattening ratio of FeSiAl particles was measured to be 1.82, showing an increment about 60 % in comparison with the initial powder (flattening ratio=1.14). These largely deformed FeSiAl particles mainly results from the two aspects - the direct impacts of deposited particles and the peening or tamping effect of subsequent particle impacts. The later factor takes an important role for particle deformation and coating densification as a large number of particles with high dynamic energy rebounding away from the coating surface, which act as in-situ peening effect on the previously deposited layers [35, 36].

Fig. 3d shows the cross-sectional view of HVOF composite coating. As indicated by the black arrows, a considerable number of pores can be clearly observed. Statistical analysis based on the cross-sectional SEM images yields a porosity level of ~1.6 %, which is much higher than that of CS coating (0.6%). Nevertheless, the porosity level in this work is much lower than the conventional HVOF sprayed FeSi alloy coatings by using the uncoated feedstocks [20]. Significant improvement in density was also reported in the HVOF deposited Ni-P coated WC-12Co coating in comparison with the conventional WC-12Co coating [37, 38]. The volumetric content of FeSiAl particles in the HVOF coating is close to 45%, being much higher than that of CS coating (25.4%). This indicates a much higher deposition efficiency of FeSiAl particles in HVOF process. Besides, it can be noticed that some big FeSiAl particles can be observed throughout the entire composite coating. The flattening ratio of FeSiAl particle was measured to be 1.24, showing slight particle deformation after HVOF deposition. As can be seen from the magnified view in Fig. 3f, apart from the well-preserved spherical FeSiAl particles, some partially melted FeSiAl traces are mixed into the Ni layers (marked by red arrows). Meanwhile, some Ni layers are mixed into the FeSiAl particles. This phenomenon can be verified by the EDS mapping result (Fig. 5). Unlike CS coating, the mixture of Ni and elements of FeSiAl phase can be found in some regions (marked by red arrows in Fig. 3 (f)) in HVOF coating. This phenomenon can be explained by the high flame temperature of HVOF process, which can lead to the partial melting of the FeSiAl particles and Ni layers. Furthermore, as revealed by the element mapping result in Fig. 5, slightly

higher oxygen content (1.2 wt.%) was detected in those partial melted regions.

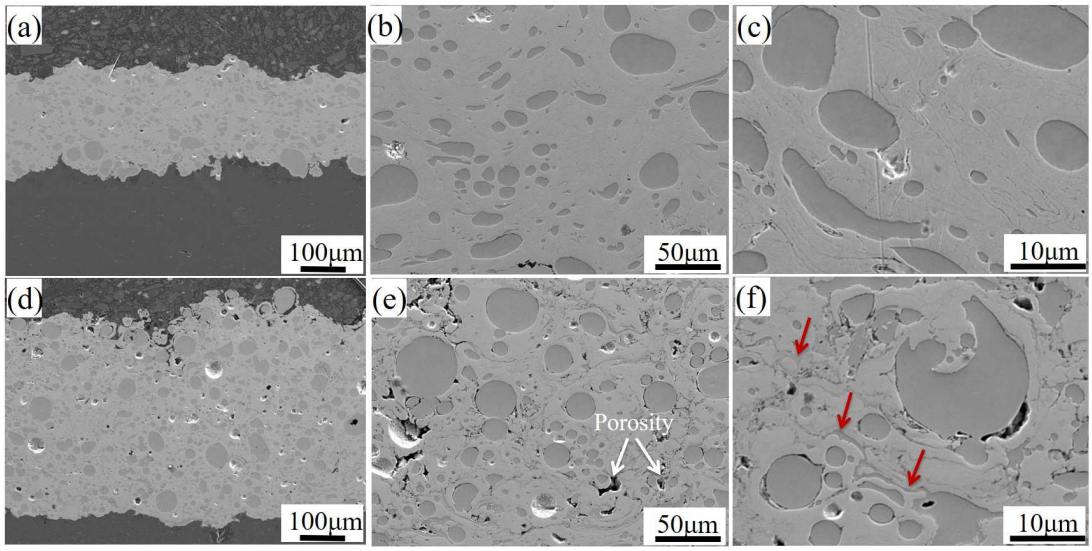

Fig. 3 SEM images of the cross sections of the CS (a-c) and HVOF composite coatings (d-f) in different magnifications.

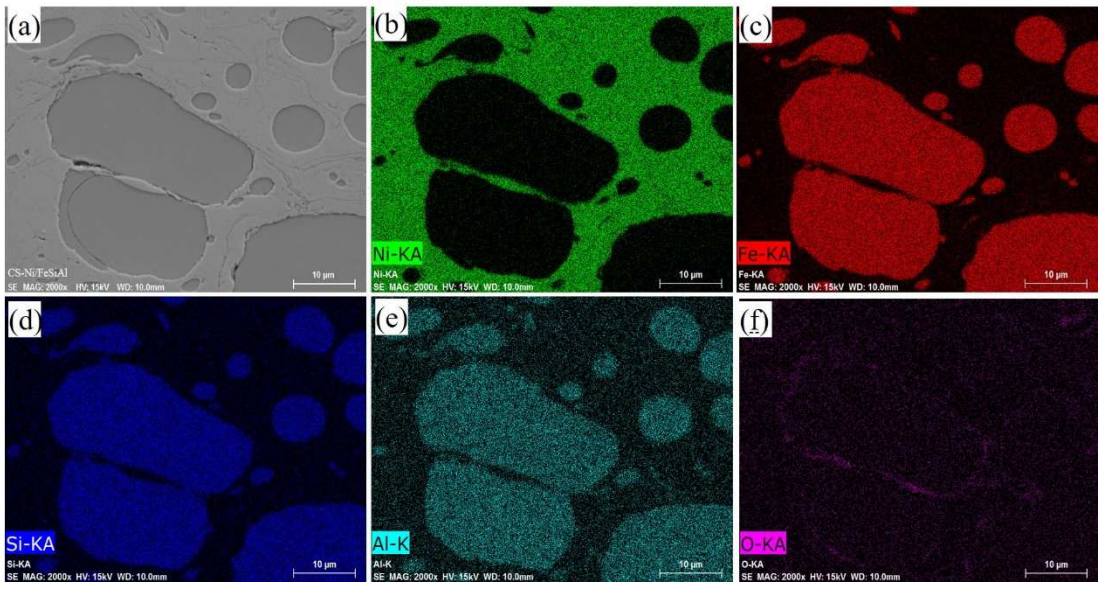

Fig. 4 SEM/EDS analysis of the cross-section of the CS composite coating.

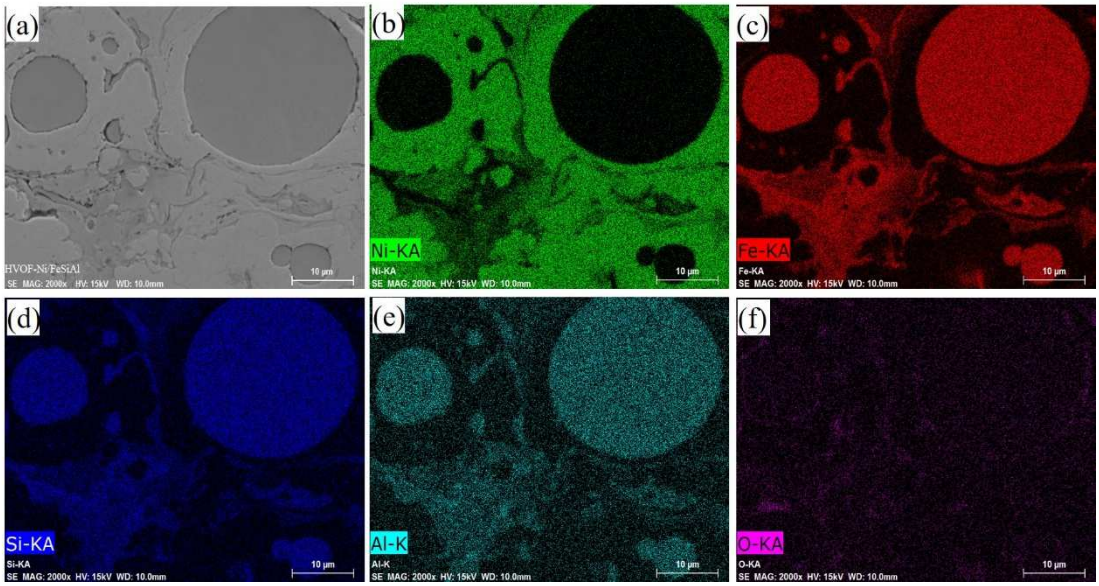

Fig. 5 SEM/EDS analysis of the cross-section of the HVOF composite coating.

Table 3 Volume fraction and flattening ratio of FeSiAl particle evolution during CS and HVOF processes.

Spray process	Volume fraction of FeSiAl in powder	Volume fraction of FeSiAl in coatings	Flattening ratio of FeSiAl particles	Microhardness of coatings ($HV_{0.3}$)
CS	62.0±1.5%	25.4±2.8%	1.82	338±32
HVOF		44.7±3.5%	1.24	268±53

3.3 Coating surface morphology

The surface morphologies of the composite coatings were displayed to further understand the microstructure evolution and deposition mechanisms. As shown in Fig. 6a, many traces of the shapes of corresponding powder particles are observed on CS coating surface. A magnified view of the particle traces is given in Fig. 6b. Considering the low retainability of FeSiAl particles, the largely deformed Ni layers in the coating surface may result from repeated hammering of the rebounding particles. As shown in Fig. 6c, a composite particle is successful bonded with the previous deposited layers by embedding into a crater. An obvious metal jet was formed for the Ni layer at the rim of the composite particle, indicating the occurrence of adiabatic shear instability [39] after severe plastic deformation

during particle impact.

Fig. 6d shows the top-view surface morphology of the HVOF composite coating. Distinct from the CS coating surface with craters and largely deformed particles, the composite particle in HVOF coating surface demonstrates a near spherical shape. Only few traces of rebounding particles can be observed, indicated by arrows in Fig. 6d. Fig. 6e displays a typical deposited composite particle, which experienced slight deformation without metal jet formation after impacting on the coating surface. However, some traces of melted particles remain on this deposited particle surface. The surface morphology in Fig. 6f also displays some melting and re-solidified regions (indicated by red dotted circle). This phenomenon is proved via EDS mapping results given in Fig. 7. These splashed traces observed on this composite particle surface is the mixture of Fe, Si, Al, Ni and O elements. It should be pointed out that the oxygen content in this melted region is about 2.3 wt.%, being much higher than the un-melted regions (1.0 wt.%).

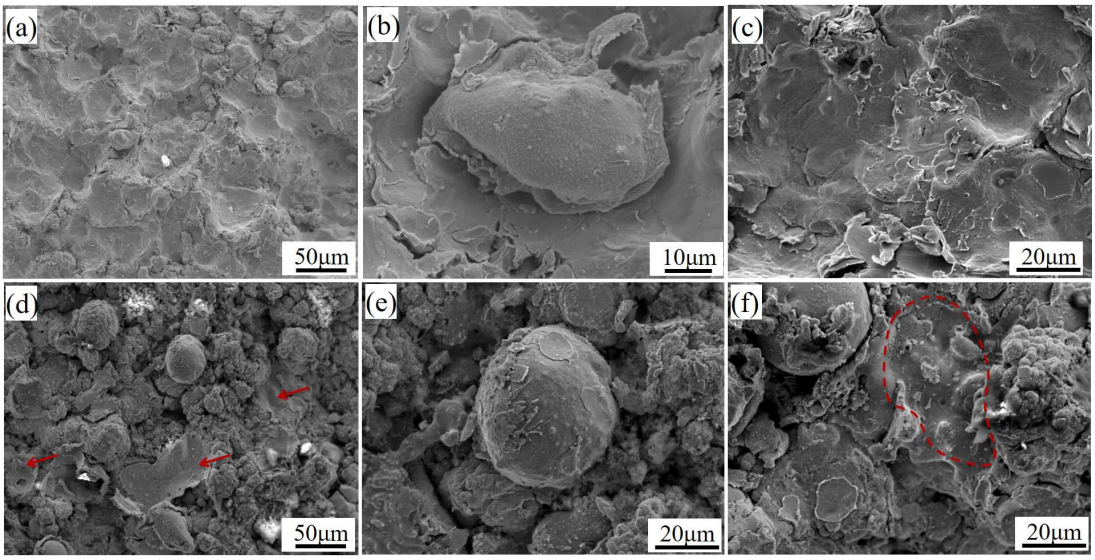

Fig. 6 Surface morphologies of the (a-c) CS and (d-f) HVOF composite coatings.

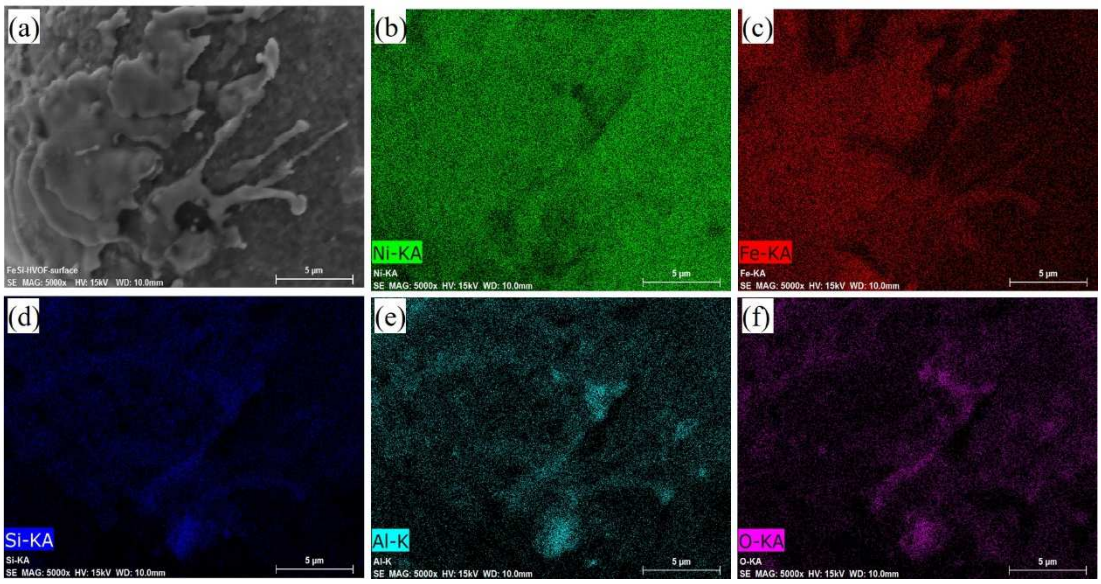

Fig. 7 SEM/EDS analysis of the coating surface of HVOF composite coating.

3.4 Deposition mechanisms

Considering the distinct coating morphology and deposition behavior, the deposition mechanisms of CS and HVOF process are then investigated in detail. Currently, the most acceptable theory of bonding mechanism in CS is considered as the mechanical interlocking and metallurgical bonding. When metallic particles impact onto metallic substrate at a high velocity, metals experience localized severe plastic deformation and the occurrence of ASI [23, 24], which will result in adiabatic heating-induced thermal softening at the particle interface [40]. The resulting outward material jets will efficiently clean the broken oxide film on the interface [41, 42], which leads to the formation of metallurgical bonding.

Previous studies have shown that hard particles decorated with a ductile layer can assist the deposition of cold sprayed coating with a high deposition efficiency [43-46]. In the case of core-shell structure powder deposition, since the core particle experienced slight plastic deformation, the ductile shell metal takes an important role in fabricating composite coating [43, 44]. In this work, during the first layer deposition, the bonding mechanism is mainly the mechanical interlocking of the composite particle onto relatively soft Al substrate, which leads to the observed large FeSiAl particles near/substrate interface (see Fig. 3a). In the subsequent deposition, the composite particles impact on the previously deposited layers with a higher hardness. The deposition mechanism of these composite particles in this stage is transformed into the metallic bonding of soft Ni layers, which experience severe plastic

deformation and thermal softening during impact [30]. The metallurgical bonding during the composite coating built-up process only takes place at the interfaces between Ni layers. When the composite particle impacts on the deposited Ni layers with sufficient thickness, the metallurgical bonding occurs between the Ni bonding layers. Conversely, the weak bonding strength between the Ni bonding layers may lead to the rebounding of the FeSiAl core or the entire Ni/FeSiAl composite particle, which caused the low retainability of FeSiAl phase in the CS composite coating. Besides, the large particles with lower impact velocity trends to rebound due to unsuccessful bonding caused by insufficient plastic deformation of Ni layer. As a result, the large particles can be hardly observed in the following deposited layers (Fig. 3a). Thus, the rebounding of FeSiAl particles attributes to the decreasing content of FeSiAl in the as-sprayed SMCs coating. These rebounded particles act as in-situ peening particles which can further enhance the plastic deformation of previous deposited layers.

Unlike CS process, in-flight particles in HVOF process gain less kinetic energy but more heat input. Generally, the in-flight particles in HVOF process can be softened or even melted as the particle temperature can reach as high as 2000 ℃ [47]. According to previous studies [48, 49], the adhesion of HVOF metallic coatings deposited by sufficiently melted spray particles was mainly determined by the mechanical interlocking effect; whereas, the deposition with the semi-molten particles can lead to the formation of physical bonding in addition to the mechanical bonding [50]. The formation of physical bonding may be resulted from the high impact pressure of the solid particles in the liquid-solid two-phase particles due to the high impact velocity during HVOF spraying [49]. Meanwhile, during the HVOF deposition of the softened particle with a solid state, the bonding mechanism should be similar to that in the CS process, where the ASI and mechanical interlocking play a key role in successful bonding. In this work, as revealed by Fig. 3d and Fig. 6d, most of the composite particles were in solid state and some small particles were partially melted during HVOF deposition. Therefore, as for these particles in solid state, the softened Ni layer can favor plastic deformation and the metallic bonding of the particles; Consequently, a higher content of FeSiAl particles was achieved in the HVOF coating compared to CS coating even through the particle impact velocity was much higher in CS process. Regarding the liquid-solid two-phase particles, the liquid fraction surrounding solid particles was forced into intimate

contact with the substrate surface or deposited layers under the substantial impact pressure of solid particle. As a result, the Van der Waals force as one of the physical bonds between the atoms in spray particle and those in the surface of substrate may occur [49]. Therefore, the physical bonding combined with mechanical interlocking may be responsible for the deposition mechanisms of the partially melted particles. More detailed research work will be carried out to look insight into the bonding mechanisms of these Ni-coated composite particles during HVOF deposition process.

Moreover, previous studies have shown that HVOF sprayed WC-Co coatings with low degree of WC decomposition were achieved using Ni-coated feedstock powders [37, 51]. In this work, the Ni-coated FeSiAl coating experienced no significant oxidation during HVOF deposition. It is suggested that the Ni layer around FeSiAl particles reduces the FeSiAl exposure to oxidizing flame, preventing direct FeSiAl oxidation and thereby evident oxide formation during HVOF process.

In summary, in the case of CS, metallic bonding can be achieved through a severe plastic deformation of the Ni layers with a high particle impact velocity. Regarding the HVOF process, the softened or even partial melted particle due to high processing temperature takes an important role in successful bonding of the composite particle.

3.5 Coating microhardness and tribological performance

The mechanical properties of the composite coatings are summarized in Table 3. In spite of a lower FeSiAl content, the CS coating shows a much higher microhardness value of ~338 $HV_{0.3}$ than that of HVOF coating (~268 $HV_{0.3}$). The higher hardness of CS coating can be explained by its low porosity, severe plastic deformation and intimate bonding of Ni layers. Owing to the high particle impact velocity as well as the enhanced in-situ peening effect, the ductile Ni layer undergoes severe plastic deformation during CS deposition. The induced plastic deformation can lead to dislocation accumulation and grain refinement for the previous deposited layers [52], which in turn results in the improvement of coating microhardness. In the case of HVOF coating, the weakened work hardening effect owing to the relative low particle deformation can result in lower microhardness.

As shown in Fig.8a, CS and HVOF coatings present a similar variation of coefficient of

friction (COF) curves. Initially, the COF increased until a peak, which can be attributed to surface asperities of the coatings. Then, the COF value decreased to reach a steady state value and remain independent of the number of cycles. During the friction process, the formation of lubricant oxide film on the coating surface can promote the stabilization of COF value. The CS coating shows a very short run-in period followed by steady state. The COF curve for HVOF coating reached steady state at a longer distance of about 50 m. The average COF value of the CS composite coating is about 0.64±0.05, which is a slightly higher than that of the HVOF coating (0.56±0.05). As shown in Fig.8b, the CS coating exhibits a smaller wear rate value than that of HVOF, which indicates a much better wear-resistance performance of CS coating. This may be due to the increased hardness in CS coating, which can enhance material resistance against plastic deformation during sliding friction. It should be noticed that both CS and HVOF composite coatings present a significantly enhanced wear performance compared to the cold sprayed Ni coating. According to Ref [53], the wear rates of the Ni/FeSiAl composite coating in this study are comparable with the cold sprayed Ni/WC composite coating which was tested under the similar conditions.

To investigate the coating wear mechanisms, the surface and cross-sectional morphologies of the worn tracks are provided in Fig. 9 and Fig. 10, respectively. For the CS composite coating, the surface morphology of worn track was characterized by smooth tribofilm with small cracks and slight material delamination. As it can be observed in Fig. 9a, there was no pulled out FeSiAl particles detected on the worn surfaces, indicative of a good cohesion between the FeSiAl particles and the Ni matrix. As it can be detected from the EDS mapping, some large FeSiAl particles were fractured during sliding but well contact with the coating. Besides, the worn surface was covered by fine fragments of fractured FeSiAl particles under the shear loading of counterparts. The fine redistributed FeSiAl particles not only facilitated the fast development of the tribolayer, improved its stability and increased hardness but also contributed to superior sliding wear resistance of the SMC coating. The cross-sectional view of the worn track is shown in Fig. 10a. A dense and crack-free tribofilm layer with a thickness of about 5-10 μm was found at the surface. The tribolayer covering the top of worn surface consisted of FeSiAl fragments detached from surfaces and

nano-crystalline Ni rich in oxygen. Such tribofilm prevented direct contact between composite coating and the ceramic counterface, thereby decreasing the wear loss of coating [53]. In addition, as marked by white arrows in Fig.10a, some cracks can be clearly observed just beneath the tribofilm, and all of these cracks were generated across the Ni phase. This fact may indicate that the material removal mechanism was probably the low-cycle fatigue of the Ni bonding phase [54].

For the HVOF coating, the worn surface showed a completely different morphology from the CS, indicating a significantly different wear mechanism. The worn surface was very rough with a large amount of delamination fractures and cracks. As shown in the EDS mapping, the exposed interior SMC coating consisting of Ni matrix and FeSiAl particles can be observed on worn track with evident fractured tribolayer and delamination. The cross-sectional view given in Fig. 10c also shows fractured tribofilms with large cracks on the coating surface. Furthermore, as it can be observed from the magnified image Fig. 10d, some large FeSiAl particles can be still noticed in the fragments of the mixed material. The tribofilm resulting from the detached plastic wear debris smears onto the worn surface, due to low toughness and tends to crack. Due to the lower microhardness values in HVOF composite coating, cracks formed easily on the tribolayer owing to localized weakening under normal and tangential loading. These initiated cracks propagate at the surface along the sliding direction, and then extend across the tribolayer, which directly leads to the observed wear flakes and delamination. Thus, the interior composite coating was exposed to the continuous sliding and friction by counterparts, which further deteriorates its wear resistance.

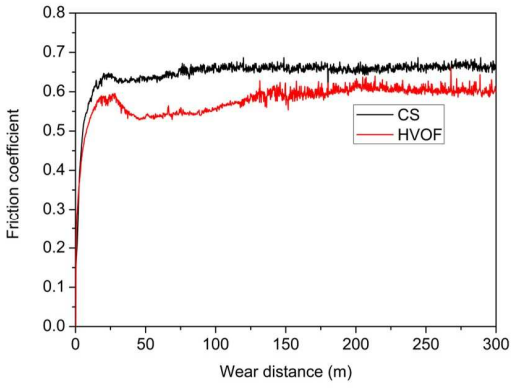

(a)

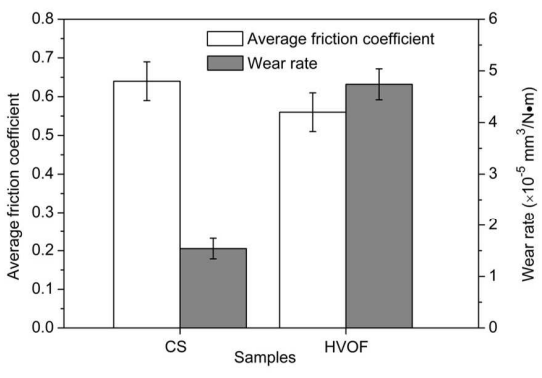

(b)

Fig. 8 (a) Friction coefficient vs. sliding wear distance and (b) average friction coefficients and wear rates of the CS and HVOF composite coatings.

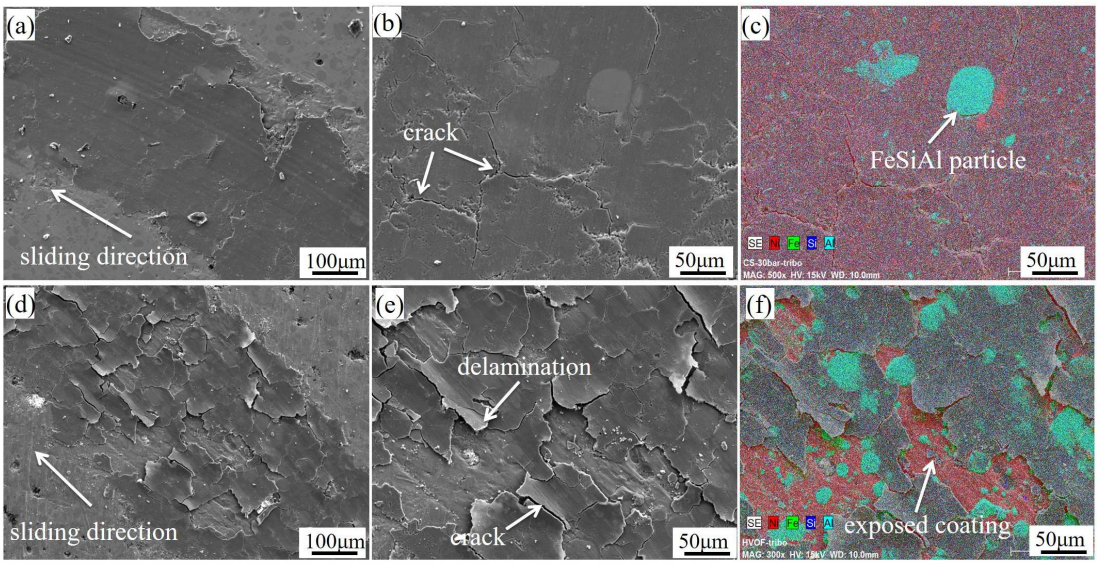

Fig. 9 Worn morphologies of (a-c) CS and (d-f) HVOF SMC coatings: (a) and (d) overview, (b) and (e) magnified view; (c) and (f) EDS mapping.

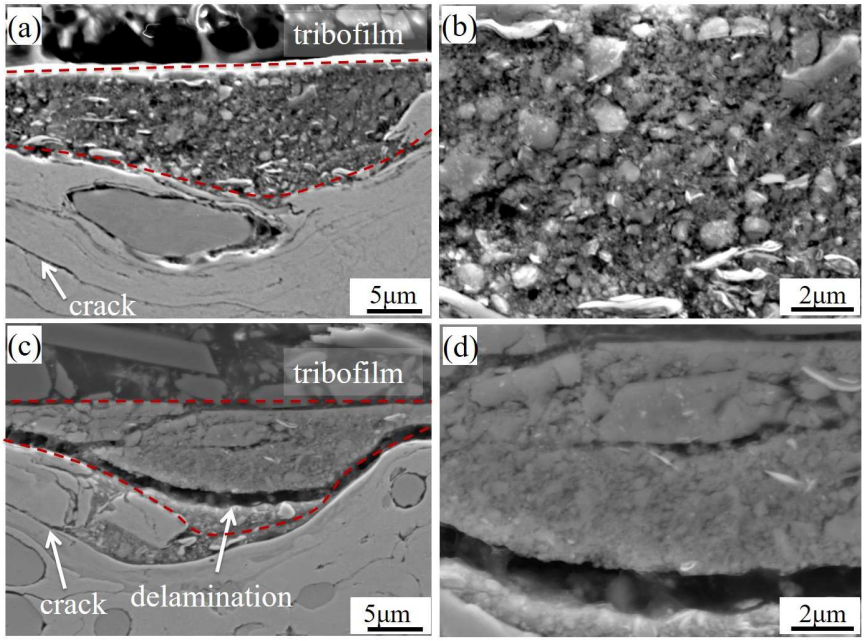

Fig. 10 Cross-sectional images of the worn coatings in different magnifications: (a) and (b) CS coating; (c) and (d) HVOF coating.

3.6 Magnetic properties

Fig.11 shows the hysteresis loops of the Ni/FeSiAl SMC coatings fabricated by CS and

HVOF process. The shapes of the hysteresis loops present low coercivities and high permeabilities, which indicates typical soft magnetic features of both coatings. Their corresponding coercivities and saturation magnetization values are given in Table. 4. The composite powder has a coercivity of 48.4 Oe and a saturation magnetization of 80.5 emu/g. After deposition, both SMC coatings show an increased coercivity and decreased saturation magnetization. One important reason for such degraded soft magnetic properties of the SMC coatings is the loss of FeSiAl particles during both deposition processes. Furthermore, the HVOF coating with a higher retainability of FeSiAl particles has a better magnetic performance, showing a lower coercivity and a higher saturation magnetization than those of the CS coating.

Besides, the generation of defects such as internal stress and dislocations in the plastic deformed FeSiAl particles and Ni layers during CS deposition can also lead to the increase of coercivity [30, 33]. As indicated by the XRD results, a higher content of internal defects was formed in the CS coating compared with the HVOF coating due to a larger plastic deformation of the particles. As a result, a smaller coercivity was obtained in the HVOF coating despite a relative high porosity and oxygen content.

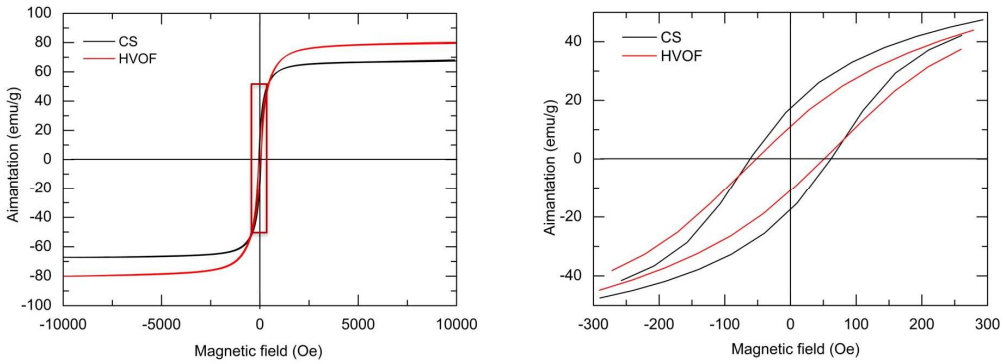

Fig. 11 Hysteresis loops of CS and HVOF composite coatings; (b) is the magnification image of (a) with the circle area.

Table 4 Coercivity and saturation magnetization of the initial powder and sprayed coatings

Sample	Coercivity Hc (Oe)	Saturation magnetization Ms (emu/g)

Powder	48.4	80.5
CS	67	68.2
HVOF	51.5	78.0

4. Conclusions

In this work, CS and HVOF techniques were employed to fabricate Ni/FeSiAl SMC coatings using Ni-coated FeSiAl composite powder. The microstructure, tribological performance and magnetic properties of the SMC coatings were comparatively investigated. The following conclusions can be drawn:

1) The CS Ni/FeSiAl composite coating exhibited a higher deformation of the particles and a much higher density, whereas the HVOF coating featured high levels of visible defects and slightly higher oxide content. Based on XRD analysis, both Ni/FeSiAl SMC coatings had no obvious phase transformation and oxide formation during deposition processes, while partial melting of FeSiAl particles were observed in the HVOF coating.

2) The Ni bonding layer plays an important role for successful deposition of the composite particles in both the CS and HVOF processes. In the case of CS process, metallic bonding can be achieved through the severe plastic deformation of the Ni layers with high particle impact velocity. The softening or partial melting of Ni layer owing to a high processing temperature should be responsible for the successful bonding during HVOF deposition as well as the higher retainability of FeiSiAl particles in the composite coating.

3) The CS composite coating had higher overall average and enhanced wear performance compared to HVOF coating due to the higher microhardness value. It can be attributed to the enhanced particle deformation and metallic bonding during CS deposition.

4) The HVOF coating displayed a better magnetic performance, with a lower coercivity and a higher saturation magnetization compared with that of the CS coating. This can

be explained by a higher retainability of FeSiAl particle and a smaller strain stress generation during HVOF deposition.

Acknowledgements

Xinliang XIE is grateful for the financial support from China Scholarship Council for his Ph.D. project.

References

[1] I. Hemmati, H.M. Hosseini, A. Kianvash, The correlations between processing parameters and magnetic properties of an iron–resin soft magnetic composite, J. Magn. Magn. Mater., 305 (2006), 147-151.
[2] R. Bensalem, W. Tebib, S. Alleg, et al., Magnetic properties of nanostructured Fe92P8 powder mixture, J. Alloys Compd., 471 (2009), 24-27.
[3] W. Li, W. Wang, J. Lv, et al., Structure and magnetic properties of iron-based soft magnetic composite with Ni-Cu-Zn ferrite–silicone insulation coating, J. Magn. Magn. Mater., 456 (2018), 333-340.
[4] M. Lauda, J. Füzer, P. Kollár, et al., Magnetic properties and loss separation in FeSi/MnZnFe 2 O 4 soft magnetic composites, J. Magn. Magn. Mater., 411 (2016), 12-17.
[5] W. Xu, C. Wu, M. Yan, Preparation of Fe–Si–Ni soft magnetic composites with excellent high-frequency properties, J. Magn. Magn. Mater., 381 (2015), 116-119.
[6] J. Li, X. Peng, Y. Yang, et al., Preparation and characterization of MnZn/FeSiAl soft magnetic composites, J. Magn. Magn. Mater., 426 (2017), 132-136.
[7] X. Jin, Q. Wang, W. Khan, et al., FeSiAl/(Ni0. 5Zn0. 5) Fe2O4 magnetic sheet composite with tunable electromagnetic properties for enhancing magnetic field coupling efficiency, J Alloy Compd, 729 (2017), 277-284.
[8] D. Liu, C. Wu, M. Yan, et al., Correlating the microstructure, growth mechanism and magnetic properties of FeSiAl soft magnetic composites fabricated via HNO 3 oxidation, Acta Mater., 146 (2018), 294-303.
[9] J. Füzer, P. Kollár, D. Olekšáková, et al., AC magnetic properties of the bulk Fe–Ni and Fe–Ni–Mo soft magnetic alloys prepared by warm compaction, J. Alloys Compd., 483 (2009), 557-559.
[10] C. Wu, H. Chen, H. Lv, et al., Interplay of crystallization, stress relaxation and magnetic properties for FeCuNbSiB soft magnetic composites, J. Alloys Compd., 673 (2016), 278-282.
[11] H. Shokrollahi, K. Janghorban, Soft magnetic composite materials (SMCs), J. Mater. Process. Technol., 189 (2007), 1-12.
[12] C. Wu, X. Gao, G. Zhao, et al., Two growth mechanisms in one-step fabrication of the oxide matrix for FeSiAl soft magnetic composites, J. Magn. Magn. Mater., 452 (2018), 114-119.
[13] R. Bai, Z. Zhu, H. Zhao, et al., The percolation effect and optimization of soft magnetic properties of FeSiAl magnetic powder cores, J. Magn. Magn. Mater., 433 (2017), 285-291.
[14] C. Oikonomou, R. Oro, E. Hryha, et al., Effect of heat treatment in air on surface composition of iron-phosphate based soft magnetic composite components, Mater. Sci. Eng.,

B, 189 (2014), 90-99.
[15] S. Dong, B. Song, X. Zhang, et al., Fabrication of FeSiB magnetic coatings with improved saturation magnetization by plasma spray and dry-ice blasting, J. Alloys Compd., 584 (2014), 254-260.
[16] B. Song, S. Dong, B. Hansz, et al., Suppression effect of decarburization by dry-ice blasting on plasma-sprayed steel coatings: Structure, wear performance and magnetic properties, Surf. Coat. Technol., 253 (2014), 44-51.
[17] E. Denisova, L. Kuzovnikova, R. Iskhakov, et al., Bulk CoNiFe-SiB Amorphous and Nanostructured Alloys Produced by Plasma Spray Deposition and Dynamic Compaction: Formation of Soft Magnetic Properties, Physics Procedia, 75 (2015), 1238-1243.
[18] X. Ni, X. Bo, J. Wu, et al., Microstructure and magnetic properties of plasma-sprayed Fe73. 5Cu1Nb3Si13. 5B9 coatings, Thin Solid Films, 519 (2011), 8287-8291.
[19] M. Cherigui, S. Guessasma, N. Fenineche, et al., Studies of magnetic properties of iron-based coatings produced by a high-velocity oxy-fuel process, Mater. Chem. Phys., 92 (2005), 419-423.
[20] M. Cherigui, N. Fenineche, G. Ji, et al., Microstructure and magnetic properties of Fe–Si-based coatings produced by HVOF thermal spraying process, J. Alloys Compd., 427 (2007), 281-290.
[21] J. Cheng, X. Liang, Y. Chen, et al., High-temperature erosion resistance of FeBSiNb amorphous coatings deposited by arc spraying for boiler applications, J. Therm. Spray Technol., 22 (2013), 820-827.
[22] M. Cherigui, N. Fenineche, C. Coddet, Structural study of iron-based microstructured and nanostructured powders sprayed by HVOF thermal spraying, Surf. Coat. Technol., 192 (2005), 19-26.
[23] M. Grujicic, C. Zhao, W. DeRosset, et al., Adiabatic shear instability based mechanism for particles/substrate bonding in the cold-gas dynamic-spray process, Mater. Des., 25 (2004), 681-688.
[24] H. Assadi, F. Gärtner, T. Stoltenhoff, et al., Bonding mechanism in cold gas spraying, Acta Mater., 51 (2003), 4379-4394.
[25] L. Ajdelsztajn, J.M. Schoenung, B. Jodoin, et al., Cold spray deposition of nanocrystalline aluminum alloys, Metall. Mater. Trans. A, 36 (2005), 657-666.
[26] D. Woo, F. Heer, L. Brewer, et al., Synthesis of nanodiamond-reinforced aluminum metal matrix composites using cold-spray deposition, Carbon, 86 (2015), 15-25.
[27] G.-J. Yang, P.-H. Gao, C.-X. Li, et al., Mechanical property and wear performance dependence on processing condition for cold-sprayed WC-(nanoWC-Co), Appl. Surf. Sci., 332 (2015), 80-88.
[28] L. Du, C. Huang, W. Zhang, et al., Effect of NiCr Clad BaF 2· CaF 2 Addition on Wear Performance of Plasma Sprayed Chromium Carbide-Nichrome Coating, J. Therm. Spray Technol., 19 (2010), 551-557.
[29] L. Du, C. Huang, W. Zhang, et al., Preparation and wear performance of NiCr/Cr3C2–NiCr/hBN plasma sprayed composite coating, Surf. Coat. Technol., 205 (2011), 3722-3728.
[30] X. Xie, C. Chen, Y. Xie, et al., A novel approach for fabricating Ni-coated FeSiAl soft magnetic composite via cold spraying, J. Alloys Compd., 749 (2018), 523-533.
[31] E.C. Santos, M. Shiomi, K. Osakada, et al., Rapid manufacturing of metal components

by laser forming, Int. J. Mach. Tool Manu., 46 (2006), 1459-1468.
[32] Y. Guo, X. Zhang, X. Feng, et al., Non-isothermal oxidation kinetics of FeSiAl alloy powder for microwave absorption at high temperature, Composites Part B, 155 (2018), 282-287.
[33] T. Ma, M. Yan, W. Wang, The evolution of microstructure and magnetic properties of Fe–Si–Al powders prepared through melt-spinning, Scripta Mater., 58 (2008), 243-246.
[34] P. Eason, S. Kennett, T. Eden, et al., In situ observation of microstrain relief in cold-sprayed bulk copper during thermal annealing, Scripta Mater., 67 (2012), 791-794.
[35] X.-T. Luo, Y.-K. Wei, Y. Wang, et al., Microstructure and mechanical property of Ti and Ti6Al4V prepared by an in-situ shot peening assisted cold spraying, Mater. Des., 85 (2015), 527-533.
[36] Y.-K. Wei, Y.-J. Li, Y. Zhang, et al., Corrosion resistant nickel coating with strong adhesion on AZ31B magnesium alloy prepared by an in-situ shot-peening-assisted cold spray, Corros. Sci., 138 (2018), 105-115.
[37] M. Jafari, M. Enayati, M. Salehi, et al., Microstructural and mechanical characterizations of a novel HVOF-sprayed WC-Co coating deposited from electroless Ni–P coated WC-12Co powders, Mater. Sci. Eng., A, 578 (2013), 46-53.
[38] M. Jafari, M. Enayati, M. Salehi, et al., Improvement in tribological properties of HVOF sprayed WC–Co coatings using electroless Ni–P coated feedstock powders, Surf. Coat. Technol., 235 (2013), 310-317.
[39] A. Papyrin, V. Kosarev, S. Klinkov, et al., Cold spray technology, Elsevier, 2006.
[40] K. Kim, M. Watanabe, S. Kuroda, Bonding mechanisms of thermally softened metallic powder particles and substrates impacted at high velocity, Surf. Coat. Technol., 204 (2010), 2175-2180.
[41] C. Chen, Y. Xie, R. Huang, et al., On the role of oxide film's cleaning effect into the metallurgical bonding during cold spray, Mater. Lett., 210 (2018), 199-202.
[42] S. Yin, X. Wang, W. Li, et al., Deformation behavior of the oxide film on the surface of cold sprayed powder particle, Appl. Surf. Sci., 259 (2012), 294-300.
[43] W.-Y. Li, C. Zhang, H. Liao, et al., Characterizations of cold-sprayed Nickel–Alumina composite coating with relatively large Nickel-coated Alumina powder, Surf. Coat. Technol., 202 (2008), 4855-4860.
[44] B. Aldwell, S. Yin, K.A. McDonnell, et al., A novel method for metal–diamond composite coating deposition with cold spray and formation mechanism, Scripta Mater., 115 (2016), 10-13.
[45] C. Feng, V. Guipont, M. Jeandin, et al., B 4 C/Ni composite coatings prepared by cold spray of blended or CVD-coated powders, J. Therm. Spray Technol., 21 (2012), 561-570.
[46] C. Huang, W. Li, M.-P. Planche, et al., In-situ formation of Ni-Al intermetallics-coated graphite/Al composite in a cold-sprayed coating and its high temperature tribological behaviors, J. Mater. Sci. Technol., 33 (2017), 507-515.
[47] X. Guo, M.-P. Planche, J. Chen, et al., Relationships between in-flight particle characteristics and properties of HVOF sprayed WC-CoCr coatings, J. Mater. Process. Technol., 214 (2014), 456-461.
[48] J. Pan, S. Hu, A. Niu, et al., Numerical analysis of particle impacting and bonding processes during high velocity oxygen fuel spraying process, Appl. Surf. Sci., 366 (2016),

187-192.
[49] Y.-Y. Wang, C.-J. Li, A. Ohmori, Influence of substrate roughness on the bonding mechanisms of high velocity oxy-fuel sprayed coatings, Thin Solid Films, 485 (2005), 141-147.
[50] C. Sun, L. Guo, G. Lu, et al., Interface bonding between particle and substrate during HVOF spraying, Appl. Surf. Sci., 317 (2014), 908-913.
[51] M. Jafari, J.-C. Han, J.-B. Seol, et al., Tribological properties of HVOF-sprayed WC-Co coatings deposited from Ni-plated powders at elevated temperature, Surf. Coat. Technol., 327 (2017), 48-58.
[52] X.-T. Luo, C.-X. Li, F.-L. Shang, et al., High velocity impact induced microstructure evolution during deposition of cold spray coatings: a review, Surf. Coat. Technol., 254 (2014), 11-20.
[53] S. Alidokht, P. Manimunda, P. Vo, et al., Cold spray deposition of a Ni-WC composite coating and its dry sliding wear behavior, Surf. Coat. Technol., 308 (2016), 424-434.
[54] S. Yin, E.J. Ekoi, T.L. Lupton, et al., Cold spraying of WC-Co-Ni coatings using porous WC-17Co powders: Formation mechanism, microstructure characterization and tribological performance, Mater. Des., 126 (2017), 305-313.

Graphical abstract